and 1.8 mm yr^{-1} with a regional average value of 0.8 mm yr^{-1}. Although this figure is somewhat higher than the trend computed without area weighting, the difference is not significant considering the poor temporal sampling found in several of the 10° × 10° areas. Thus, we conclude that area weighting is not essential to this study. The formal uncertainties of trends of dynamic height derived from 5-yr means are 0.1–0.2 mm yr^{-1}. These are smaller than the uncertainty values from gauge data because the former are based on area averages.

Except for the Balboa area, which suffers from relatively poor temporal sampling, the hydrographic results presented in Fig. 2 are not overly sensitive to the size or orientation of the sample areas. Cutting the width of the California area in half, that is, setting the offshore boundary at 220 km instead of 440 km as shown, results in a dynamic height trend of 0.4 mm yr^{-1} instead of 0.5 mm yr^{-1} over 1938–1996. Similarly, cutting the Honolulu area in half results in a dynamic height trend of 0.4 mm yr^{-1} instead of 0.3 mm yr^{-1} from 1950 to 1999.

Received 15 July; accepted 22 December 2003; doi:10.1038/nature02309.

1. Church, J. A. *et al. Climate Change 2001: The Scientific Basis* (ed. Houghton, J. T.) Ch. 11 (Cambridge Univ. Press, New York, 2001).
2. Douglas, B. C. & Peltier, W. R. The puzzle of global sea level rise. *Phys. Today* **55**(3), 35–40 (2002).
3. Munk, W. Twentieth century sea level: an enigma. *Proc. Natl Acad. Sci. USA* **99,** 6550–6555 (2002).
4. Meier, M. & Wahr, J. M. Sea level is rising: do we know why? *Proc. Natl Acad. Sci. USA* **99,** 6524–6526 (2002).
5. Munk, W. Ocean freshening, sea level rising. *Science* **300,** 2041–2043 (2003).
6. Cabanes, C., Cazenave, A. & LeProvost, C. Sea level rise during past 40 years determined from satellite and in situ observations. *Science* **294,** 840–842 (2001).
7. Antonov, J. I., Levitus, S. & Boyer, T. P. Steric sea level variations 1957–1994: importance of salinity. *J. Geophys. Res.* **107,** doi:10.1029/200/JC000964 (2002).
8. Levitus, S., Antonov, J. I., Boyer, T. P. & Stephens, C. Warming of the world ocean. *Science* **287,** 2225–2229 (2000).
9. Warrick, R. A., Le Provost, C., Meier, M. F., Oerlemans, J. & Woodworth, P. L. in *Climate Change 1995, The Science of Climate Change* (eds Houghton, J. T. *et al.*) 359–405 (Cambridge Univ. Press, Cambridge, 1996).
10. Nerem, R. S. & Mitchum, G. T. in *Sea Level Rise; History and Consequences* (eds Douglas, B. C., Kearney, M. S. & Leatherman, S. P.) 65–95 (Academic, San Diego, 2001).
11. Ducet, N., Le Traon, P. Y. & Reverdin, G. Global high-resolution mapping of ocean circulation from TOPEX/Poseidon and ERS-1 and -2. *J. Geophys. Res. C* **105,** 19477–19498 (2002).
12. World Ocean Atlas 1998v2. ⟨http://www.nodc.noaa.gov/OC5/wod98v2.html⟩
13. Joyce, T. M., Deser, C. & Spall, M. A. The relation between decadal variability of Subtropical Mode Water and the North Atlantic Oscillation. *J. Clim.* **13,** 2550–2569 (2000).
14. Permanent Service for Mean Sea Level ⟨http://www.pol.ac.uk/psmsl/psmsl_individual_stations.html⟩ (accessed 2003).
15. Peltier, W. R. in *Sea Level Rise; History and Consequences* (eds Douglas, B. C., Kearney, M. S. & Leatherman, S. P.) 65–95 (Academic, San Diego, 2001).

Acknowledgements We thank G. Mitchum for comments and suggestions; T. Rossby, P. Woodworth, S. Gille, R. Cheney, J. Lillibridge, W. Smith and B. Miller for insights; and C. Y. Kuo and C. K. Shum for sharing their computations based on the WOA98 interpolated data set. This work was supported in part by NOAA's Climate Services and Observations Program and NASA. The views, opinions, and findings contained in this report are those of the authors, and should not be construed as an official NOAA or US Government position, policy or decision.

Competing interests statement The authors declare that they have no competing financial interests.

Correspondence and requests for materials should be addressed to L.M. (laury.miller@noaa.gov).

Experimental evidence for the existence of iron-rich metal in the Earth's lower mantle

Daniel J. Frost[1], Christian Liebske[1], Falko Langenhorst[1], Catherine A. McCammon[1], Reidar G. Trønnes[1,2] & David C. Rubie[1]

[1]*Bayerisches Geoinstitut, University of Bayreuth, D-95440 Bayreuth, Germany*
[2]*Nordic Volcanological Institute, Natural Sciences Building, University of Iceland, IS-101, Reykjavík, Iceland*

The oxidation state recorded by rocks from the Earth's upper mantle can be calculated from measurements of the distribution of Fe^{3+} and Fe^{2+} between the constituent minerals[1–3]. The capacity for minerals to incorporate Fe^{3+} may also be a significant factor controlling the oxidation state of the mantle[4,5], and high-pressure experimental measurements of this property might provide important insights into the redox state of the more inaccessible deeper mantle. Here we show experimentally that the Fe^{3+} content of aluminous silicate perovskite, the dominant lower-mantle mineral, is independent of oxygen fugacity. High levels of Fe^{3+} are present in perovskite even when it is in chemical equilibrium with metallic iron. Silicate perovskite in the lower mantle will, therefore, have an Fe^{3+}/total Fe ratio of at least 0.6, resulting in a whole-rock ratio of over ten times that of the upper mantle[5,6]. Consequently, the lower mantle must either be enriched in Fe^{3+} or Fe^{3+} must form by the disproportionation of Fe^{2+} to produce Fe^{3+} plus iron metal. We argue that the lower mantle contains approximately 1 wt% of a metallic iron-rich alloy. The mantle's oxidation state and siderophile element budget have probably been influenced by the presence of this alloy.

The Earth's upper mantle contains both ferric and ferrous iron but ferrous iron is by far the more dominant species ($Fe^{3+}/\Sigma Fe < 0.03$) (refs 5, 6). Chemical equilibria between Fe^{3+}- and Fe^{2+}-bearing minerals in mantle rocks can be used to calculate the oxygen fugacity of the upper mantle, which is generally found to fall within +1 and −2 log units of the quartz–fayalite–magnetite oxygen buffer[1–3]. This lower bound is more than three orders of magnitude above the level where the upper mantle would be in chemical equilibrium with metallic iron, as probably occurred during core–mantle segregation.

The oxygen fugacity of an upper-mantle assemblage equates quite reasonably with the concentration of Fe^{3+} in some constituent minerals. The Fe^{3+} content of spinel, for example, decreases with decreasing oxygen fugacity towards zero at conditions of equilibrium with metallic iron[3]. This relationship is dependent on mineral structure and chemistry, however, and at higher pressures there are examples of silicate minerals (such as wadsleyite, ringwoodite and majoritic garnet) that have significant Fe^{3+} concentrations when coexisting with metallic iron[4,5]. The crystal–chemical constraints that make Fe^{2+} the dominant iron species in the upper mantle may not, therefore, hold for the transition zone and lower mantle, where mixtures of Fe^{3+}-rich minerals and metallic Fe may become stable, even if bulk oxygen contents are the same as in the upper mantle.

Using a multianvil high-pressure apparatus, we have synthesized samples of aluminous silicate perovskite coexisting with metallic Fe to determine the $Fe^{3+}/\Sigma Fe$ ratio of perovskite under these relatively reducing conditions. Aluminous pyroxene starting materials were ground with an additional 20 wt% powdered metallic Fe and equilibrated in Fe capsules at 1,600 °C for run durations of up to five days. In most experiments 20 wt% ferropericlase was also added. Additional experiments in graphite capsules using a synthetic peridotite composition, without added metallic Fe, were performed at conditions slightly below and above the silicate solidus. The $Fe^{3+}/\Sigma Fe$ ratios of silicate perovskite in the recovered samples were measured using Mössbauer and electron energy loss spectroscopy[7] and are reported in Table 1. Figure 1a shows a typical run product. In addition to using a Fe capsule, distributing metallic Fe throughout the experimental charge is essential for ensuring redox equilibrium between the silicate and metal.

Figure 2 shows the Fe^{3+} versus the Al^{3+} content of perovskite in atoms per two-cation formula unit for samples equilibrated with metallic Fe at typical mantle temperatures. The shaded region encompasses results with uncertainties from similar experiments performed under more oxidizing conditions in the presence of Re and ReO_2 (refs 8, 9). The Fe^{3+} content of perovskite is coupled to the Al^{3+} concentration[8–10]. The nonlinear relationship between Al^{3+} and Fe^{3+} may result from a gradual change in the dominant trivalent cation incorporation mechanism—from one involving oxygen vacancies at low Al^{3+} concentrations, to a coupled substitution of trivalent cations at higher Al^{3+} concentrations[9]. Computer simulations indicate that such a coupled substitution remains favourable at least up to 100 GPa, that is, over most of the lower

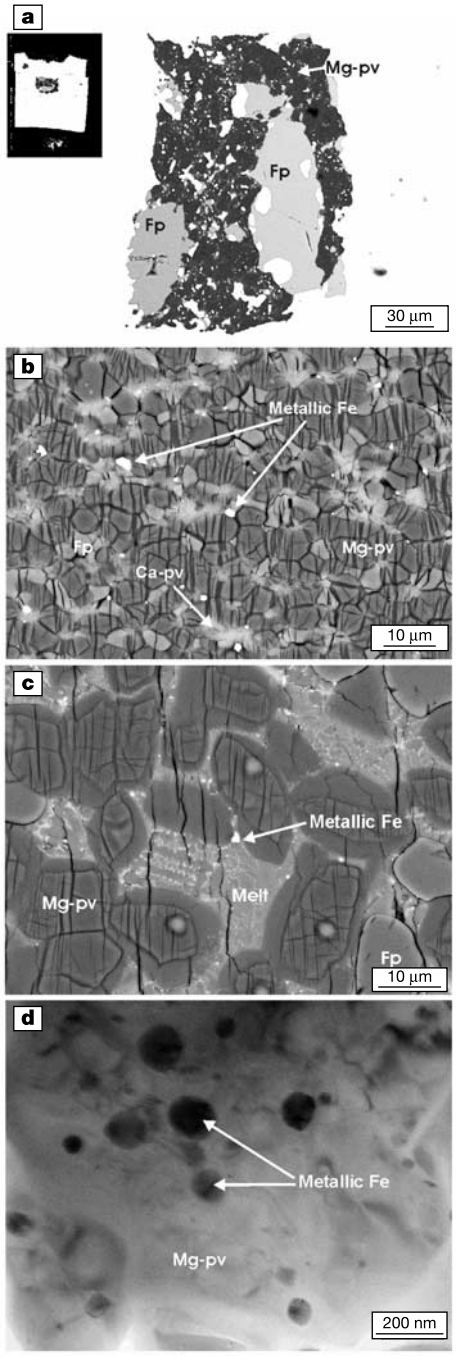

Figure 1 Scanning (**a**–**c**) and transmission (**d**) electron microscope images of experimental run products. **a**, An iron capsule containing magnesium silicate perovskite (Mg-pv) and ferropericlase (Fp). Bright metallic Fe powder, which was added to the starting material, can be seen throughout the sample. Inset, the entire capsule rotated 90°. The capsule is 0.8 mm in diameter. An Al_2O_3 sleeve surrounded the Fe capsule inside the multianvil high-pressure assembly. **b**, A sub-solidus run product in a diamond capsule. Grains of magnesium silicate perovskite, calcium perovskite (Ca-pv) and ferropericlase (Fp) can be seen with small amounts of metallic Fe that formed during the experiment. Metallic Fe was not added to these starting materials. **c**, A super-solidus experiment run in a diamond capsule where magnesium silicate perovskite and silicate melt can be seen with a grain of metallic Fe that must also have formed during the experiment. **d**, A TEM image of a cluster of submicrometre-sized particles of metallic Fe inside ferric iron-rich magnesium silicate perovskite (run 2002).

mantle[11]. Our new data indicate that the relationship between Al^{3+} and Fe^{3+} is independent of oxygen fugacity because the Fe^{3+} content of perovskite in equilibrium with metallic Fe is very similar to the level measured under more-oxidizing conditions. The oxygen fugacity of the Re–ReO_2 buffer is approximately 6 log units above the metallic Fe equilibrium. At oxygen fugacities slightly lower than those investigated here, all Fe in the system would be reduced to metal. Experiments performed above the silicate solidus also demonstrate that perovskite has a significant Fe^{3+} concentration during either crystallization or partial melting (Fig. 2).

If the lower mantle has a typical bulk silicate earth composition[12,13], then it will be composed of approximately 70 wt% silicate perovskite, which will contain around 5 wt% Al_2O_3 (refs 14, 15). Using our Fe^{3+} versus Al^{3+} relationship, we calculate that perovskite in the lower mantle must have an $Fe^{3+}/\Sigma Fe$ ratio of approximately 0.6. This means that either the lower mantle is enriched in Fe^{3+} compared to the upper mantle, or that silicate perovskite appropriates oxygen either by the reduction of volatile species or by the disproportionation of Fe^{2+} to Fe^{3+} and metallic Fe.

The first possibility is inconsistent with evidence for whole-mantle convection[16]. The redox state of the upper mantle seems to have remained relatively constant since 3.6 Gyr ago[17,18], which would not have occurred if there were significant mixing with an Fe^{3+}-rich lower mantle. The second possibility implies that the bulk oxygen content of the lower mantle is the same or similar to the upper mantle and that oxidation of Fe^{2+} to Fe^{3+} is balanced by reduction of some other component. Volatile species such as H_2O and CO_2 could be reduced to diamond, CH_4 and H_2 in order to release oxygen, but the mantle budget of CO_2 and H_2O together is probably only of the order of 2,000 p.p.m. at most[19], so such a reduction could only account for a fraction of the required oxygen. Several studies have also proposed that in deeper regions of the upper mantle and transition zone these volatile species are already in a reduced state[5,20,21]. The most realistic scenario, therefore, is for oxygen to be provided by the reduction of Fe^{2+} to metallic iron:

$$3FeO \rightarrow Fe + Fe_2O_3 \quad (1)$$

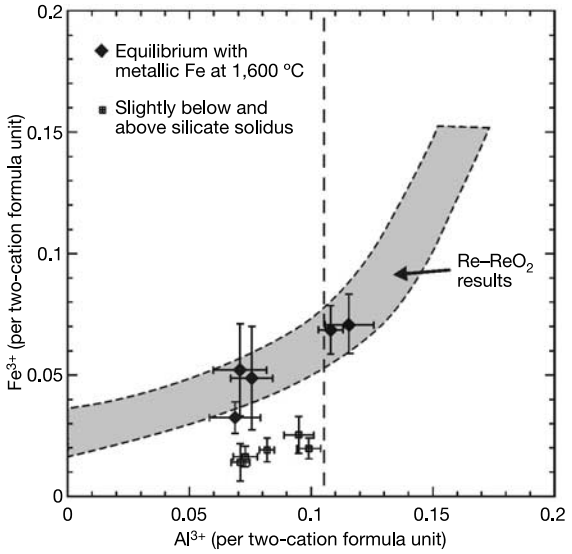

Figure 2 The variation of Al^{3+} and Fe^{3+} in silicate perovskite reported as atoms per two-cation formula unit. Analyses from experiments performed in equilibrium with metallic Fe at a typical temperature for the top of the lower mantle (1,600 °C) are shown as black diamonds. The grey field encompasses analyses from experiments performed at a higher oxygen fugacity in equilibrium with the Re–ReO_2 buffer[8,9]. Analyses of perovskites forming slightly below and above the silicate solidus (~2,200 °C) are shown as small squares. The vertical dotted line indicates the approximate Al content of silicate perovskite expected in a lower mantle with a typical bulk silicate earth composition[12,13].

Table 1 **Experimental conditions and perovskite compositions**

Run number	Pressure (GPa)	Temperature (°C)	Time (h)	$Fe^{3+}/\Sigma Fe \times 100$	Si	Al	Fe^{3+}	Fe^{2+}	Mg	Ca
Fe capsules with Fe metal powder added to the starting material										
202	24	1,600	120	48 (5) E	0.927 (10)	0.069 (10)	0.032 (6)	0.035 (7)	0.937 (27)	–
218a	24	1,600	96	35 (15) M	0.922 (11)	0.076 (11)	0.051 (22)	0.094 (22)	0.858 (19)	–
218b	24	1,600	96	37 (16) M	0.923 (69)	0.075 (8)	0.049 (21)	0.083 (21)	0.869 (14)	–
2002	26	1,600	24	68 (10) E	0.897 (16)	0.115 (9)	0.071 (11)	0.034 (8)	0.884 (23)	–
2014	26	1,600	7	66 (10) M	0.898 (11)	0.108 (5)	0.069 (10)	0.035 (10)	0.889 (11)	–
Graphite capsules with no added Fe metal powder										
3224	24	2,150	2	20 (11) M	0.939 (6)	0.071 (4)	0.014 (8)	0.056 (8)	0.887 (9)	0.020 (7)
3242*	24	2,300	0.2	30 (9) M	0.901 (8)	0.095 (6)	0.025 (8)	0.059 (8)	0.884 (11)	0.025 (2)
				46 (10) E	0.91	0.099	0.020	0.023	0.916	0.025
				39 (10) E	0.93	0.073	0.016	0.026	0.927	0.024
				39 (10) M	0.926 (8)	0.082 (3)	0.019 (5)	0.030 (5)	0.911 (11)	0.024 (4)

Letters after $Fe^{3+}/\Sigma Fe$ values refer to the analysis technique that is either electron energy loss (E) or Mössbauer (M) spectroscopy. Electron microprobe analyses are normalized to a two-cation formula unit (for example, $MgSiO_3$). Minor amounts of Ti, Cr, Ni, Mn and Na are excluded from the perovskite compositions of experiments 3224 and 3242.
*As a result of the thermal gradient experiment 3242 encompassed a range of conditions from sub-solidus to the silicate liquidus. Analyses were made at various points along this regime. The first two analyses are from a region close to the solidus, whereas the second two are from regions containing silicate melt.

The observation that high levels of Fe^{3+} can occur in perovskite in equilibrium with metallic Fe means that Fe^{2+} disproportionation must occur if aluminous perovskite is formed in a system that is initially poor in Fe^{3+}. The formation of aluminous perovskite with the appropriate Fe^{3+} content from a bulk silicate earth[12,13] composition with an initial $Fe^{3+}/\Sigma Fe$ ratio similar to the upper mantle[5,6] requires the precipitation of approximately 1 wt% metallic Fe-rich alloy. The alloy would contain approximately 88 wt% Fe, 10 wt% Ni, and 1 wt% S together with the majority of the lower mantle's siderophile elements. The Ni content, calculated using 25 GPa partition coefficients[22], may decrease with pressure[23]. Although the perovskite Fe^{3+} concentration is slightly lower at the silicate solidus (Fig. 2), approximately 0.5 wt% alloy would still be expected to form at these conditions.

Circumstantial evidence in support of disproportionation can be found in experiments performed on peridotite compositions in diamond capsules. Powdered metallic Fe was not added to these experiments but Fe-rich metal has formed in equilibrium with aluminous silicate perovskite (Fig. 1b, c). Transmission electron microscope images also indicate the formation of submicrometre metal inclusions (Fig. 1d).

This proportion of metal is unlikely to have separated from the solid lower mantle even at temperatures above the metal solidus as a consequence of the high interfacial energies between Fe-rich liquid metal and lower-mantle minerals[24,25]. During mantle convection, Fe^{2+} in descending material entering the lower mantle would disproportionate to exsolve metal, which would remain locked in the silicate assemblage. As material ascended out of the stability field of perovskite, Fe^{3+} and metal would recombine to Fe^{2+}, retaining the same bulk oxygen content. Such a metal phase would probably evade geophysical detection. A metallic phase of this proportion would not significantly influence the electrical conductivity of the lower mantle because it would not be interconnected. In fact, experiments have shown aluminous and ferric iron-rich perovskite to have an electrical conductivity quite consistent with that of the lower mantle[26]. This amount of metal would also be too small to measurably influence seismic wave velocities in the lower mantle. The Fe^{3+} content may influence the elastic properties of silicate perovskite, however, which should be taken into consideration when comparing lower-mantle seismic velocities with experimentally and theoretically determined values.

The formation of the metallic phase in the lower mantle has important implications for the evolution of the redox state of the mantle. Core–mantle segregation would have ensured that the early silicate mantle was more reduced than present-day upper mantle[27,28]. Irrespective of whether silicate perovskite formed by solid-state transformation during accretion or by crystallization from a magma ocean, disproportionation of Fe^{2+} would have occurred concurrently because the precursor material would have been poor in Fe^{3+}. Iron-rich metal must, therefore, have existed in the lower mantle from the moment silicate perovskite became stable and could not have separated to a large extent without creating a lower mantle enriched in oxygen.

Many accretion models propose that core-forming liquid metal descended through the solid lower mantle[23,28,29]. In this case, the descending metal could have transported some of the disproportionated metal into the core. Transport of the metal to the core could also have been aided by the formation of a deep magma ocean from which metal would exsolve as aluminous silicate perovskite crystallized. This would result in a net increase in the oxygen content of the lower mantle and after convection the bulk oxygen content of the mantle would be raised. This is consistent with the observation that the upper mantle today is more oxidized than it was likely to have been during core formation[5,28]. To increase the $Fe^{3+}/\Sigma Fe$ ratio of the upper mantle to its present-day level, from that expected during core formation, requires of the order of 10% of the disproportionated metal phase to segregate into the core.

If a solid lower mantle were in place before the completion of core formation, then the metallic phase could have retained a significant quantity of siderophile elements that would have otherwise been extracted to the core. Subsequent homogenization of the mantle by convection might then help to explain why many siderophile elements are over-abundant in the upper mantle in comparison to their expected behaviour during core–mantle differentiation[30]. If correct, this eliminates the necessity for a chondritic 'late veneer'[27] in geochemical accretion models. □

Received 4 November 2003; accepted 17 February 2004; doi:10.1038/nature02413.

1. O'Neill, H. St C. & Wall, V. J. The olivine-orthopyroxene-spinel oxygen geobarometer, the nickel precipitation curve, and the oxygen fugacity of the Earth's upper mantle. *J. Petrol.* **28,** 1169–1191 (1987).
2. Luth, R. W., Virgo, D., Boyd, F. R. & Wood, B. J. Ferric iron in mantle derived garnets: implications for thermobarometry and the oxidation state of the mantle. *Contrib. Mineral. Petrol.* **104,** 56–72 (1990).
3. Ballhaus, C., Berry, R. F. & Green, D. H. High pressure experimental calibration of the olivine-orthopyroxene-spinel oxygen geobarometer: implications for the oxidation state of the upper mantle. *Contrib. Mineral. Petrol.* **107,** 27–40 (1991).
4. O'Neill, H. St C. *et al.* Mössbauer spectroscopy of mantle transition zone phases and determination of minimum Fe^{3+} content. *Am. Mineral.* **78,** 456–460 (1993).
5. O'Neill, H. St C. *et al. Ferric Iron in the Upper Mantle and in Transition Zone Assemblages: Implications for Relative Oxygen Fugacities in the Mantle* Vol. 14, 73–89 (Geophys. Monogr. 74, International Union of Geodesy and Geophysics (IUGG), Washington DC, 1993).
6. Canil, D. & O'Neill, H. St C. Distribution of ferric iron in some upper-mantle assemblages. *J. Petrol.* **37,** 609–635 (1996).
7. van Aken, P. A., Liebscher, B. & Styrsa, V. S. Quantitative determination of iron oxidation states in minerals using Fe L2,3-edge electron energy-loss near-edge structure spectroscopy. *Phys. Chem. Mineral.* **5,** 323–327 (1998).
8. Lauterbach, S., McCammon, C. A., van Aken, P., Langenhorst, F. & Seifert, F. Mössbauer and ELNES spectroscopy of $(Mg,Fe)(Si,Al)O_3$ perovskite: a highly oxidised component of the lower mantle. *Contrib. Mineral. Petrol.* **138,** 17–26 (2000).

9. Frost, D. J. & Langenhorst, F. The effect of Al_2O_3 on Fe-Mg partitioning between magnesiowüstite and magnesium silicate perovskite. *Earth Planet. Sci. Lett.* **199,** 227–241 (2002).
10. McCammon, C. Perovskite as a possible sink for ferric iron in the lower mantle. *Nature* **387,** 694–696 (1997).
11. Richmond, N. C. & Brodholt, J. P. Calculated role of alumina in the incorporation of ferric iron into magnesium silicate perovskite. *Am. Mineral.* **83,** 947–951 (1998).
12. McDonough, W. F. & Sun, S.-s. The composition of the Earth. *Chem. Geol.* **120,** 223–253 (1995).
13. O'Neill, H. S. C. & Palme, H. in *The Earth's Mantle* (ed. Jackson, I.) 3–126 (Cambridge Univ. Press, Cambridge, 1998).
14. Irifune, T. Absence of an aluminous phase in the upper part of the lower mantle. *Nature* **370,** 131–133 (1994).
15. Kesson, S. E., Fitz Gerald, J. D. & Shelley, J. M. Mineralogy and dynamics of a pyrolite lower mantle. *Nature* **392,** 252–255 (1998).
16. van der Hilst, R. D., Widiyantoro, S. & Engdahl, E. R. Evidence for deep mantle circulation from global tomography. *Nature* **386,** 578–584 (1997).
17. Canil, D. Vanadium partitioning and the oxidation state of Archaean komatiite magmas. *Nature* **389,** 842–845 (1997).
18. Delano, J. W. Redox history of the Earth's interior since ~3900 Ma: Implications for prebiotic molecules. *Orig. Life Evol. Biosph.* **31,** 311–341 (2001).
19. Wood, B. J., Pawley, A. & Frost, D. J. Water and carbon in the Earth's mantle. *Phil. Trans. R. Soc. Lond. A* **354,** 1495–1511 (1996).
20. Ballhaus, C. Is the upper-mantle metal-saturated? *Earth Planet. Sci. Lett.* **132,** 75–86 (1995).
21. Ballhaus, C. & Frost, B. R. The generation of oxidized CO_2-bearing basaltic melts from reducing CH_4-bearing upper-mantle sources. *Geochim. Cosmochim. Acta* **58,** 4931–4940 (1994).
22. Asahara, Y., Kubo, T. & Kondo, T. Phase relations of a carbonaceous chondrite at lower mantle conditions. *Phys. Earth Planet. Inter.* (in the press).
23. Walter, M. J., Newsom, H. E., Ertel, W. & Holzheid, A. in *Origin of the Earth and Moon* (eds Canup, R. & Righter, K.) 285–289 (Univ. Arizona Press, Tucson, 2000).
24. Shannon, M. C. & Agee, C. B. Percolation of core melts at lower mantle conditions. *Science* **280,** 1059–1061 (1998).
25. Agee, C. B. & Shannon, M. C. Experimental constraints on percolative core formation at lower mantle conditions. *Lunar Planet. Sci. Abstr.* **XXVIII,** 7 (1997).
26. Xu, Y. S., McCammon, C. & Poe, B. T. The effect of alumina on the electrical conductivity of silicate perovskite. *Science* **282,** 922–924 (1998).
27. O'Neill, H. S. C. The origin of the Moon and the early history of the Earth—A chemical model. Part 2: The Earth. *Geochim. Cosmochim. Acta* **55,** 1159–1172 (1991).
28. Righter, K., Drake, M. J. & Yaxley, G. Prediction of siderophile element metal-silicate partition coefficients to 20 GPa and 2,800 °C: the effect of pressure, temperature, fo_2 and silicate and metallic melt composition. *Phys. Earth Planet. Inter.* **100,** 115–134 (1997).
29. Stevenson, D. J. in *Origin of the Earth* (eds Newsom, H. E. & Jones, J. H.) 231–249 (Oxford Univ. Press, Oxford, 1990).
30. Ringwood, A. E. Chemical evolution of the terrestrial planets. *Geochim. Cosmochim. Acta* **30,** 41–104 (1966).

Acknowledgements We thank H. Fischer, G. Herrmannsdörfer, D. Krausse and H. Schulze for technical assistance. The German Science Foundation (DFG) and the EU Access to Research Infrastructures Programme supported this research.

Competing interests statement The authors declare that they have no competing financial interests.

Correspondence and requests for materials should be addressed to D.J.F. (dan.frost@uni-bayreuth.de).

Antibiotic-mediated antagonism leads to a bacterial game of rock–paper–scissors *in vivo*

Benjamin C. Kirkup & Margaret A. Riley

Department of Ecology and Evolutionary Biology, Yale University, New Haven, Connecticut 06511, USA

Colicins are narrow-spectrum antibiotics produced by and active against *Escherichia coli* and its close relatives. Colicin-producing strains cannot coexist with sensitive or resistant strains in a well-mixed culture, yet all three phenotypes are recovered in natural populations[1]. Recent *in vitro* results conclude that strain diversity can be promoted by colicin production in a spatially structured, non-transitive interaction[2], as in the classic non-transitive model rock–paper–scissors (RPS). In the colicin version of the RPS model, strains that produce colicins (C) kill sensitive (S) strains, which outcompete resistant (R) strains, which outcompete C strains. Pairwise *in vitro* competitions between these three strains are resolved in a predictable order (C beats S, S beats R, and R beats C), but the complete system of three strains presents the opportunity for dynamic equilibrium[2]. Here we provide conclusive evidence of an *in vivo* antagonistic role for colicins and show that colicins (and potentially other bacteriocins) may promote, rather than eliminate, microbial diversity in the environment.

Colicins are high-molecular-mass bacteriocins produced by *E. coli*[3,4]. *In vitro* experiments show that coexistence of a colicin producer and a sensitive strain in a well-mixed culture is not possible[5–7]. In natural populations a further phenotype, colicin-resistant, is always present, and more recent *in vitro* and *in silico* work has incorporated this third phenotype[2,6,8,9]. Theoretical and empirical studies reveal that a combination of colicinogenic, sensitive and resistant provides a stabilizing factor in a mixed, spatially structured assemblage[2,6,8]. This complex of three strains has the same formal structure as the RPS game[2], with C beating S (by killing), S beating R (by growth-rate advantage, because the resistant strain has had to modify a receptor used in nutrient uptake), and R beating C (because colicin production involves bacterial suicide). Thus, these authors conclude that antagonistic factors, such as colicins, may promote biological diversity in natural microbial populations and communities[2].

Colicins have repeatedly been the subject of *in vivo* studies that failed to confirm expectations generated by laboratory and mathematical studies for potent antagonism[4,10]. However, whereas those studies generally regarded resistance as a nuisance phenomenon, the RPS model treats it as central to the establishment of a dynamic equilibrium. To validate this new model of colicin-related population dynamics, a new *in vivo* experimental model was applied. Controlled enteric bacterial populations were established in small populations of mice so that the bacterial population dynamics could be monitored as bacteria migrated from mouse to mouse.

This mouse model has proved to be highly effective in studies of enteric bacteria in the mammalian colon[11]. Streptomycin eliminates from the mouse colon the minority Gram-negative microbial community, which is replaced with the desired streptomycin-resistant Gram-negative test strains. The majority Gram-positive communities remain relatively undisturbed[12,13], and the mouse experiences normal colon development and function[11,14].

To study the impact of colicins on bacterial dynamics in this mouse model, four related *E. coli* strains were generated. The base strain, *E. coli* K12 (BZB1011), is naturally sensitive to most known colicins. A streptomycin-resistant mutant of BZB1011 was selected as the colicin-sensitive (S) strain. Two colicin-producing strains (C_{E1} and C_{E2}) were derived by introducing naturally occurring colicin plasmids into the S strain by electroporation. These two colicins (E1 and E2) were chosen because they represent colicins commonly found in mouse colon isolates, are encoded on easily manipulated, non-transformable, low-molecular-mass plasmids, and act in distinctly different ways. Colicin E2 is a DNase that enters the cell and nonspecifically cleaves DNA[15]. In contrast, colicin E1 produces voltage-gated pores in the cell membrane, depolarizing the cell[15]. To produce the fourth strain, S was exposed to colicin E2, and a resistant strain (R) was isolated. This strain was resistant to both colicin E1 and colicin E2. DNA sequencing of the *btuB* locus of the R strain suggests that the resistance phenotype was generated by an IS1 insertion (J. E. Wertz and C. Winkworth, personal communication).

Seventy-two mice were given streptomycin in their drinking water. The sensitive and resistant *E. coli* were inoculated by mouth into 24 mice each, and C_{E1} and C_{E2} were inoculated into 12 mice each. In all cases the new strains rapidly colonized their hosts, and all achieved final densities of about 10^6 colony-forming units per gram of faeces, similar to the frequency of enteric bacteria